Supplementary Information (SI) for Journal of Materials Chemistry C.
This journal is © The Royal Society of Chemistry 2024

# CoNi-bimetallic Coordination Polymers as Catalyst for Boosting Oxygen Evolution Reaction Activity

Jia Du*[ab], Xueguo Liu[a], Meng Guo[a], Bingke Li[a], Hongyong Ye[a], Lixuan Chen[a]

* Corresponding author. E-mail address: 3132085@nyist.edu.cn

a. School of Biology and Chemical Engineering, Nanyang Institute of Technology, No.80, Changjiang Road, Nanyang 473000, Henan, People's Republic of China.

b. Key Laboratory of Advanced Energy Materials Chemistry (Ministry of Education), College of Chemistry, Nankai University, Tianjin 300071, People's Republic of China.

## Experimental

### 1. Materials

All the chemicals and solvents were of analytical grade and employed without further purification. Cobalt(II) acetate tetrahydrate ($Co(OAc)_2 \cdot 4H_2O$, 99.5%) was purchased from Shanghai Aladdin Biochemical Technology Co. Ltd. Nickel (II) acetate tetrahydrate ($Ni(OAc)_2 \cdot 4H_2O$, 99%) was purchased from J&K Scientific. 2,5-dihydroxy-3,6-dichlorobenzene quinone ($H_2CA$, 98%) was purchased from Shanghai Macklin Biochemical Co., Ltd. The 5% Nafion solution was purchased from Beijing InnoChem Science & Technology Co., Ltd.

### 2. Sample preparation

Synthesized of Co-CA: 0.2 mmol $Co(OAc)_2 \cdot 4H_2O$ was weighed and dissolved in the mixed solution of 6 mL methanol and 2 mL water, denoted as solution A. 0.1 mmol $H_2CA$ was dissolved in a mixed solution of 4 mL methanol and 4 mL water, denoted as solution B. The solution A was added to the solution B drop by drop under stirring, and the mixed solution was continued to stir for 30 min after the titration was finished and then left for 3 days. The obtained dark red product was filtered and washed with 20 mL distilled water for 3 times respectively.

Synthesized of Ni-CA: the same method was applied for synthesizing Ni-CA expect for a substitution from $Co(OAc)_2 \cdot 4H_2O$ to $Ni(OAc)_2 \cdot 4H_2O$.

Synthesized of $Co_xNi_{1-x}$-CAs: For the synthesis of $Co_xNi_{1-x}$-CAs (x = 4/5, 2/3, 1/2, 1/3, 1/5), the same method was applied for synthesizing Co-CA expect for different ratios between Co and Ni were controlled by adjusting the amounts of $Co(OAc)_2 \cdot 4H_2O$ and $Ni(OAc)_2 \cdot 4H_2O$.

## 3. Characterization

Powder X-ray diffraction (PXRD) data were recorded on a Rigaku MiniFlex600 diffractometer by Cu-Ka radiation at $5^o$ $min^{-1}$ and the measurement range was from $5.0^o$ to $60^o$ ($2\theta$) with a step of $0.020^o$ ($2\theta$). The single-crystal X-ray diffraction measurements of Co-CA was recorded on an Agilent Technologies Supernova diffractometer using graphite-monochromatized Mo Kα radiation ($\lambda$ = 0.71073 Å). Thermal gravimetric analysis (TGA) data were conducted by a METILER TOLEDO TCA/DSC1 apparatus at a heating rate of 10 ºC $min^{-1}$ from 40 to 800ºC. Fourier transform infrared (FT-IR) spectra were conducted in the wavenumber of 400-4000 $cm^{-1}$ on a PerkinElmer Spectrum Two infrared spectrophotometer at room temperature under $N_2$ atmosphere. Scanning electron microscopy (SEM) images and EDS mapping images were obtained on a JEOL JSM-7900F scanning electron microscope. $N_2$ sorption analysis was performed on a SSA-4300 instrument with liquid nitrogen temperature (77 K). Transmission electron microscopy (TEM) images were obtained on a FEI Tecnai G2F20 electron microscope. A Thermo Fisher K-alpha was employed to conduct X-ray photoelectron spectroscopy (XPS) and the binding energies were normalized by the C 1s peak at 284.6 eV with an Al Kα X-ray source (hν = 1486.6 eV). The content of Co and Ni in $Co_xNi_{1-x}$-CAs was measured by an elementar Vario EL cube inductively coupled plasma-optical (ICP) emission spectrometer.

## 4. Electrochemical measurements

Electrochemical measurements were conducted via a three-electrode system by an electrochemical workstation (CHI 760E, ChenHua Instruments Co.) within 1 M KOH solution.

A glassy carbon (GC) electrode with a diameter of 3 mm was applied as the working electrode; an Ag/AgCl (saturated KCl) electrode and a platinum sheet electrode were applied as the reference and counter electrodes. All the electrocatalyst inks were prepared by dispersing the corresponding sample (3 mg) and Nafion solutions (5 wt%, 40 μL) into DMF (960 μL) and followed with a 30 min ultrasonic treatment. 7 μL of the catalyst ink was dropped onto the polished GC electrode with a mass loading of 0.30 mg $cm^{-2}$ and then dried overnight at RT. All the measured potentials were converted to the reversible hydrogen electrode (RHE) based on the Nernst equation ($E_{RHE} = E_{Ag/AgCl} + 0.059$ pH $+ 0.197$ V). The overpotential ($\eta$) of OER was obtained from the following formula: $\eta = E_{RHE} - 1.23$ V. The linear sweep voltammetry (LSV) curves were recorded at a scan rate of 5 mV $s^{-1}$. Tafel slopes were determined from the LSV curves. By fitting the linear portion of the Tafel plots, the TS was acquired according to the Tafel equation of g = b log (j) + a. The double layer capacitance was calculated for the determination of electrochemically active surface area ECSA analysis by the CV scans in a non-Faradaic potential range of as-prepared catalysts electrodes in 1 M KOH at a scan rate of 10 to 100 mV/s. Half of the differences in current density variation (ΔJ = (Janodic-Jcathodic)/2) at a potential of 1.16 V vs RHE plotted against scan rate fitted to a linear regression that allows the determination of double layer capacitance ($C_{dl}$). Turnover frequency (TOF) was calculated based on the equation of TOF = J × A / (z × F × n), where J is the measured current density at a certain potential, A is the electrode area, z is the number of electrons for the oxidation of one molecule (4 for OER, F is the Faraday constant, and n is the moles of active sites on the electrode. Co and Ni contents were obtained from ICP results (Table S2). The electrochemical impedance spectroscopy (EIS) tests were conducted at a potential of 0.5 V vs. Ag/AgCl electrode, with an amplitude of 5.0 mV in a frequency range of 0.1–$10^6$ Hz. The faradic efficiency was determined by calculating the ratio of the experimental and theoretical oxygen evolution. The amount of oxygen bubbles evolved from the $Co_{1/2}Ni_{1/2}$-CA catalyst was observed after initiating electrolysis and the fluorescence-based oxygen sensor showed a rise of the oxygen percentage in the headspace with the increase of passed charge. The time points at every 5 min of collected $O_2$ gas were recorded. The quantity of oxygen produced during this time was determined by converting its concentration to mol using the ideal gas law. The accumulated charges passing through the working electrode were recorded using electrochemical workstation under a fixed current of 10 mA for 30 min by the equation (Q=It). The faradaic yield was calculated from the total amount of charges passed through the cell and the total amount of oxygen produced, assuming that four electrons are needed to produce one $O_2$ molecule.

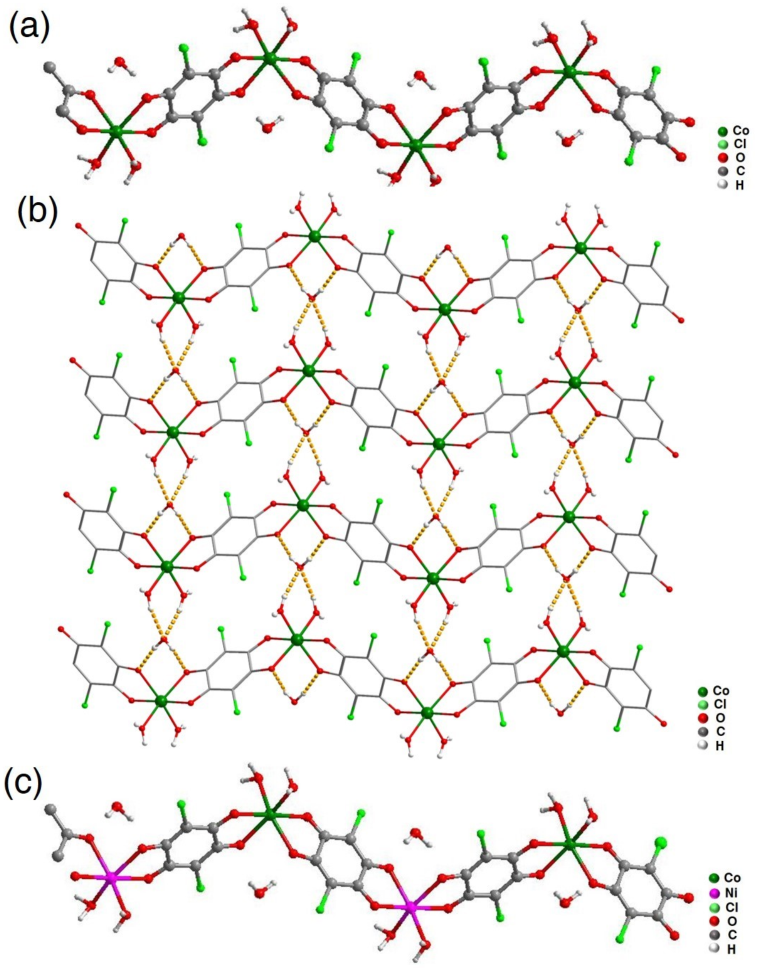

**Fig. S1.** Crystal structure of (a) Co-CA and (b) Co$_{1/2}$Ni$_{1/2}$-CA, (c) three-dimensional supramolecular framework of Co-CA.

Utilizing the single crystal data of Co-CA and the bibliographical data published enclosed on the Cambridge Structural Database (CSD),[S1-S2] each Co center is coupled to four O atoms from two adjacent CA$^{2-}$ ligands, while the remaining coordination sites are occupied by two $H_2O$ molecules, producing an environment that is octahedral (Table S1). A chain structure is produced by CA$^{2-}$ and metal center linkage in succession (Fig. S1a). A three-dimensional supramolecular framework is generated by hydrogen interactions between $H_2O$ molecules and the oxygen in ligands (Fig. S1b). Through manipulation of the Co/Ni molar ratio, a range of metal-mixed coordination polymers Co$_x$Ni$_{1-x}$-CAs were synthesized to enhance the electrocatalytic activity. PXRD patterns (Fig. 1b) reveal that all the synthesized Co$_x$Ni$_{1-x}$-CAs are isostructural to the Co-CA with high phase purity. FTIR spectra of the isostructural Co-CA and Co$_x$Ni$_{1-x}$-CAs are similar as well (Fig. 1c). Further, according to ICP emission spectrometer and EDS analysis (Table S2), the Co/Ni molar ratios of Co$_x$Ni$_{1-x}$-CAs match well with the feeding molar ratios.

According to the experimental results of ICP and EDS, we simulated the structure diagram of $Co_{1/2}Ni_{1/2}$-CA refer to Co-CA, as shown in Fig. S1c. Each Co or Ni center is connected to three O atoms from two $CA^{2-}$ ligands, and other coordination sites are taken up by three $H_2O$ molecules, forming an octahedral environment. The alternating connection of $CA^{2-}$ and metal centers lead to a chain structure. The central metallic framework of the compound features an even dispersion of cobalt and nickel, with each individual element occupying an equal portion. The structural configuration of other $Co_xNi_{1-x}$-CAs is theoretically analogous to that of Co-CA, with the exception being the transition from pure cobalt to varying compositions of cobalt and nickel at the metal center.

**Table S1.** Data collection and processing parameters for Co-CA.

| | Co-CA |
|---|---|
| formula | $C_9H_9CoN_2O_6$ |
| Formula weight | 300.11 |
| Temperature/K | 293(2) |
| Crystal system | Orthorhombic |
| Space group | Pbca |
| a/Å | 11.9856(5) |
| b/Å | 11.1121(4) |
| c/Å | 15.6900(4) |
| α/° | 90 |
| β/° | 90 |
| γ/° | 90 |
| Volume/Å$^3$ | 2089.68(13) |
| Z | 8 |
| $\rho_{calc}$g/cm$^3$ | 1.908 |
| μ/mm$^{-1}$ | 1.667 |
| F(000) | 1216.0 |
| Crystal size/mm$^3$ | 0.08 × 0.06 × 0.04 |
| Radiation | MoKα (λ = 0.71073) |
| 2Θ range for data collection/° | 5.192 to 61.17 |
| Index ranges | $-16 \leq h \leq 16$, $-14 \leq k \leq 15$, $-22 \leq l \leq 19$ |
| Reflections collected | 11488 |
| Independent reflections | 3099 [$R_{in}$ = 0.0256, $R_{sigma}$ = 0.0267] |
| Data/restraints/parameters | 3099/0/172 |
| Goodness-of-fit on F$^2$ | 0.942 |
| Final R indexes [I>=2σ (I)] | $R_1$ = 0.0300, $wR_2$ = 0.0765 |
| Final R indexes [all data] | $R_1$ = 0.0401, $wR_2$ = 0.0817 |
| Largest diff. peak/hole / e Å$^{-3}$ | 0.40/-0.49 |

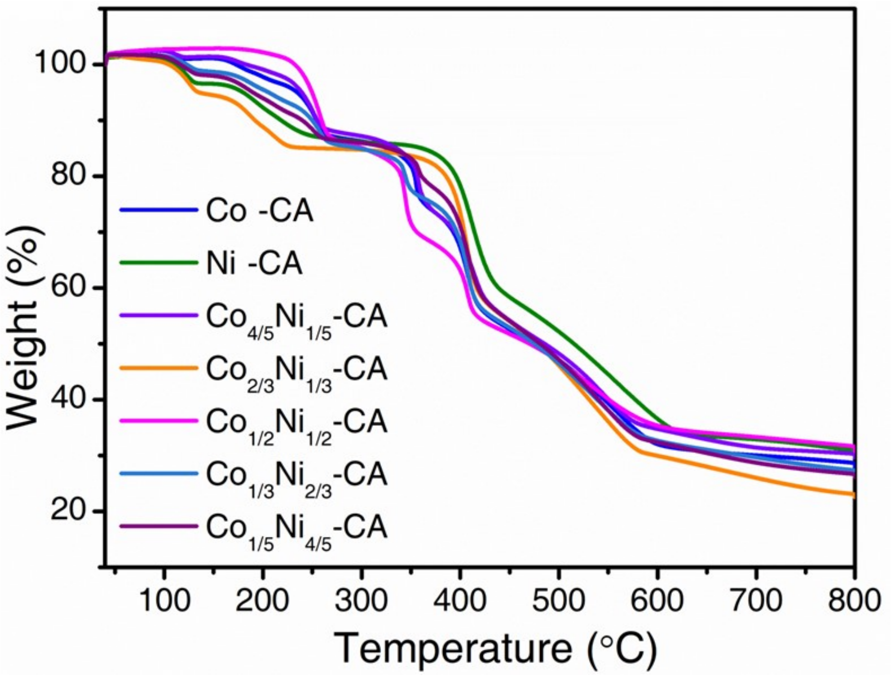

**Fig. S2.** TGA of $Co_xNi_{1-x}$-CAs.

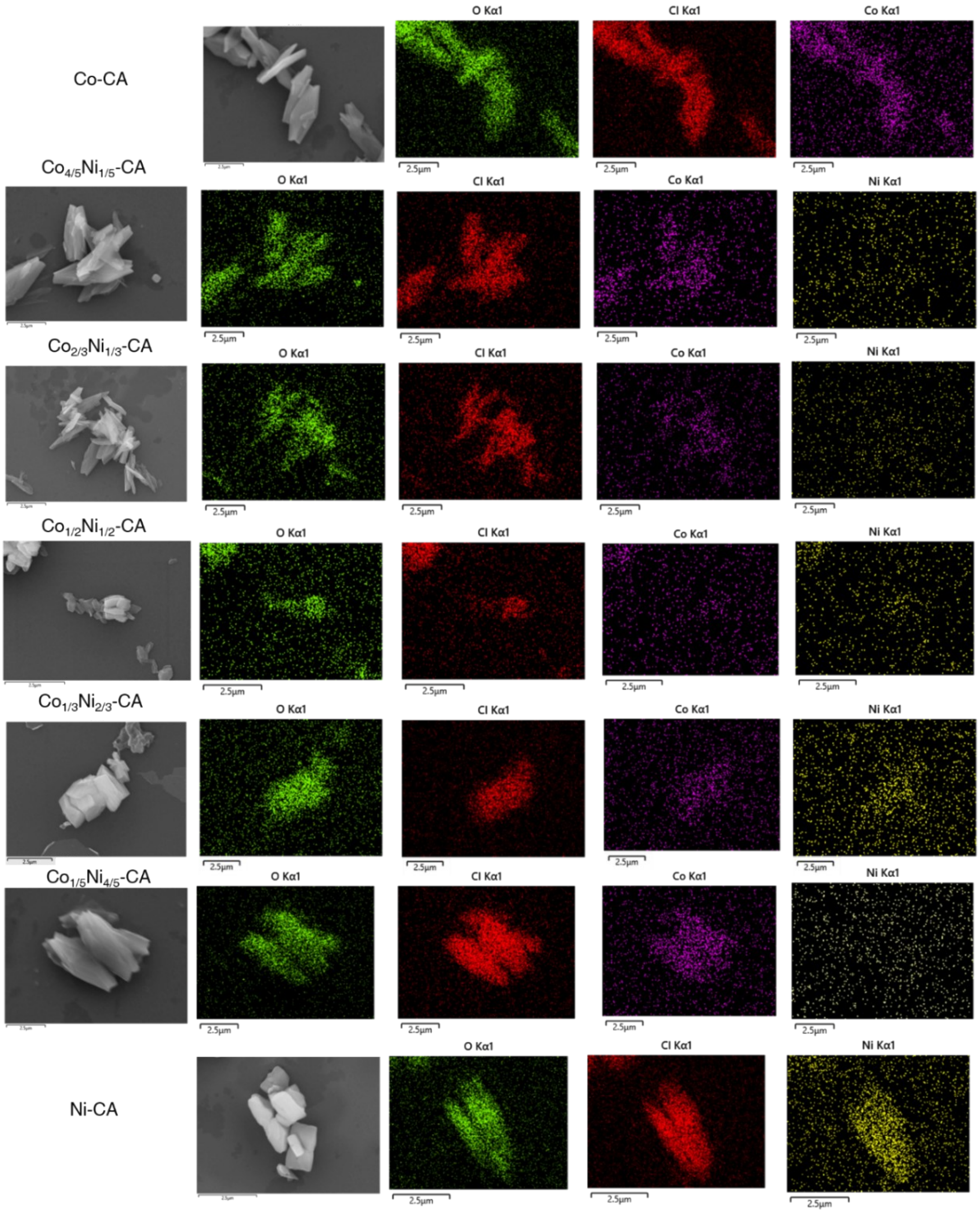

**Fig. S3.** SEM and EDS images of Co-CA (a), $Co_{4/5}Ni_{1/5}$-CA (b), $Co_{2/3}Ni_{1/3}$-CA (c), $Co_{1/2}Ni_{1/2}$-CA (d), $Co_{1/3}Ni_{2/3}$-CA (e), $Co_{1/5}Ni_{4/5}$-CA (b) and Ni-CA (f).

**Table S2**. ICP and EDS data of $Co_xNi_{1-x}$-CAs (x = 0, 4/5, 2/3, 1/2, 1/3, 1/5, 1).

| sample | ICP measured Co content (wt%) | ICP measured Ni content (wt%) | ICP measured molar ratio (Co : Ni) | EDS measured molar ratio (Co : Ni) |
|---|---|---|---|---|
| Co-CA | 19.64 | -- | -- | -- |
| $Co_{4/5}Ni_{1/5}$-CA | 16.55 | 4.25 | 0.80 : 0.20 | 0.84 : 0.16 |
| $Co_{2/3}Ni_{1/3}$-CA | 13.52 | 6.42 | 0.68: 0.32 | 0.70 : 0.30 |
| $Co_{1/2}Ni_{1/2}$-CA | 9.79 | 10.02 | 0.49 : 0.51 | 0.46 : 0.54 |
| $Co_{1/3}Ni_{2/3}$-CA | 7.03 | 13.21 | 0.35 : 0.65 | 0.36 : 0.64 |
| $Co_{1/5}Ni_{4/5}$-CA | 4.56 | 15.39 | 0.23 : 0.77 | 0.18 : 0.72 |
| Ni-CA | 19.67 | -- | -- | -- |

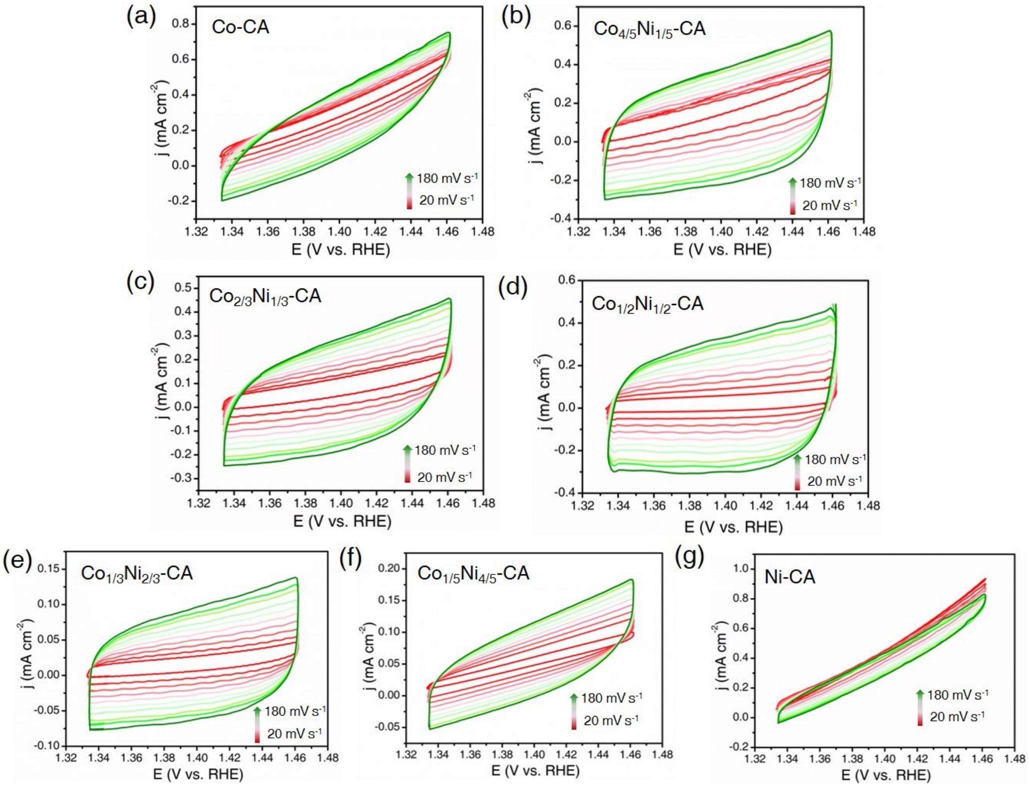

**Fig. S4.** CV curves of Co-CA (a), $Co_{4/5}Ni_{1/5}$-CA (b), $Co_{2/3}Ni_{1/3}$-CA (c), $Co_{1/2}Ni_{1/2}$-CA (d), $Co_{1/3}Ni_{2/3}$-CA (e), $Co_{1/5}Ni_{4/5}$-CA (f) and Ni-CA (g) at 25 °C.

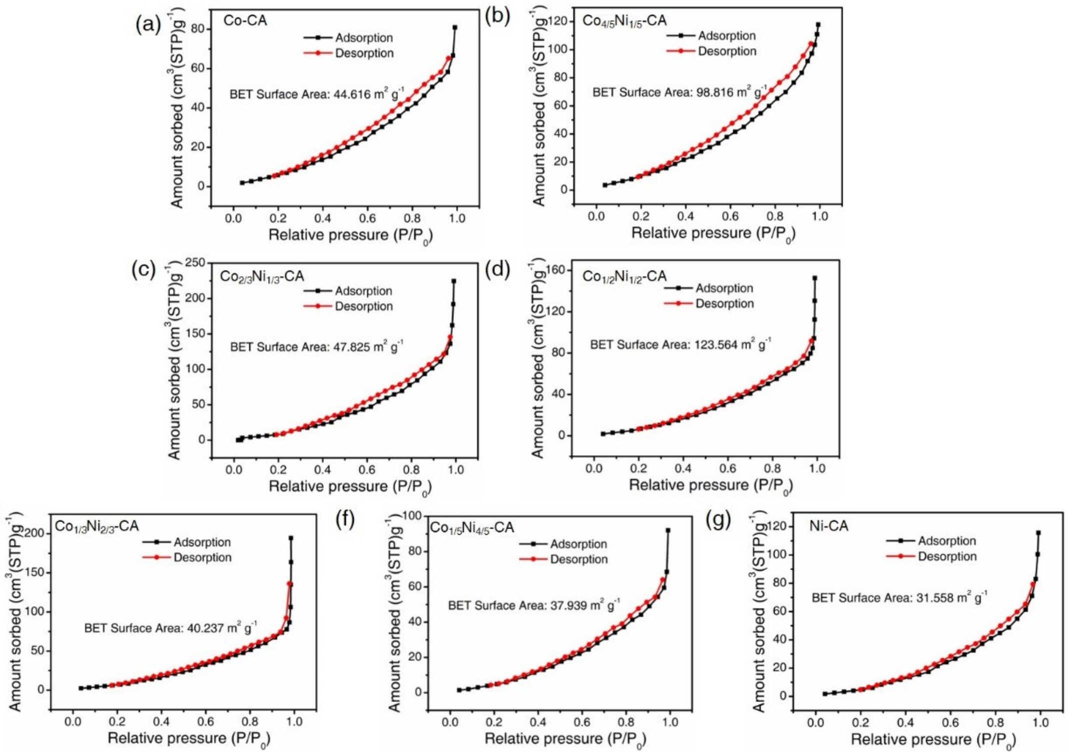

**Fig. S5.** $N_2$ adsorption/desorption isotherms of Co-CA (a), $Co_{4/5}Ni_{1/5}$-CA (b), $Co_{2/3}Ni_{1/3}$-CA (c), $Co_{1/2}Ni_{1/2}$-CA (d), $Co_{1/3}Ni_{2/3}$-CA (e), $Co_{1/5}Ni_{4/5}$-CA (f) and Ni-CA (g).

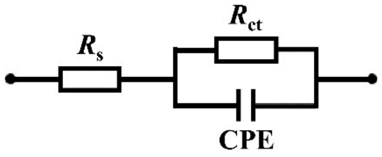

**Fig. S6.** The equivalent circuit of Nyquist plot.

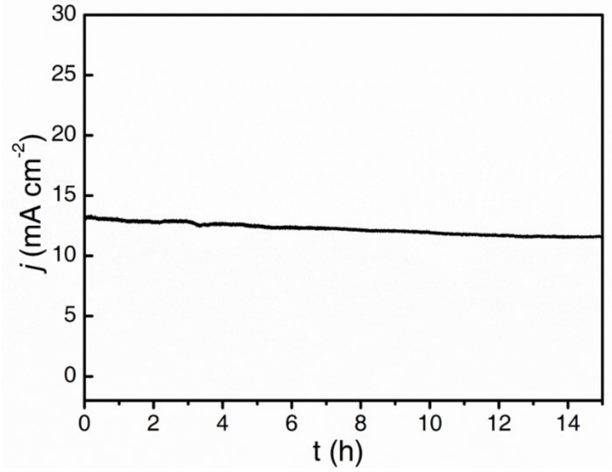

**Fig. S7.** Chronoamperometric curve of $Co_{1/2}Ni_{1/2}$-CA.

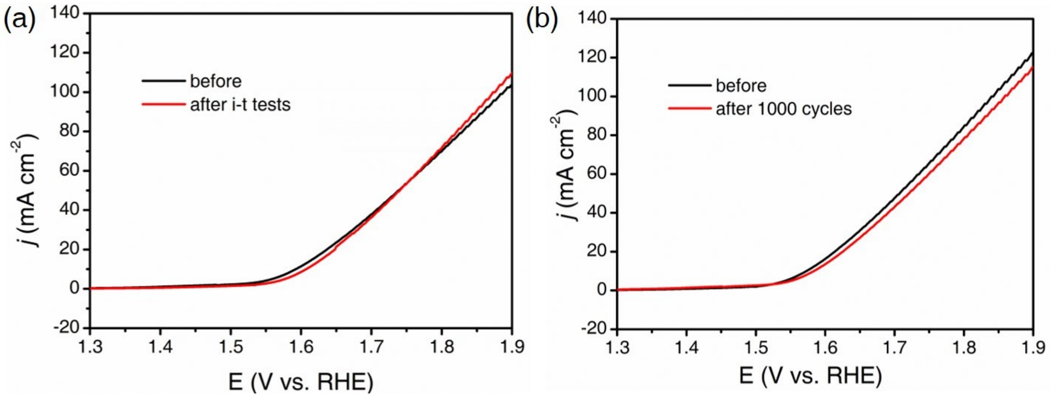

**Fig. S8.** LSV before and after chronoamperometric test (a) and 1000 CV cycles (b) of $Co_{1/2}Ni_{1/2}$-CA.

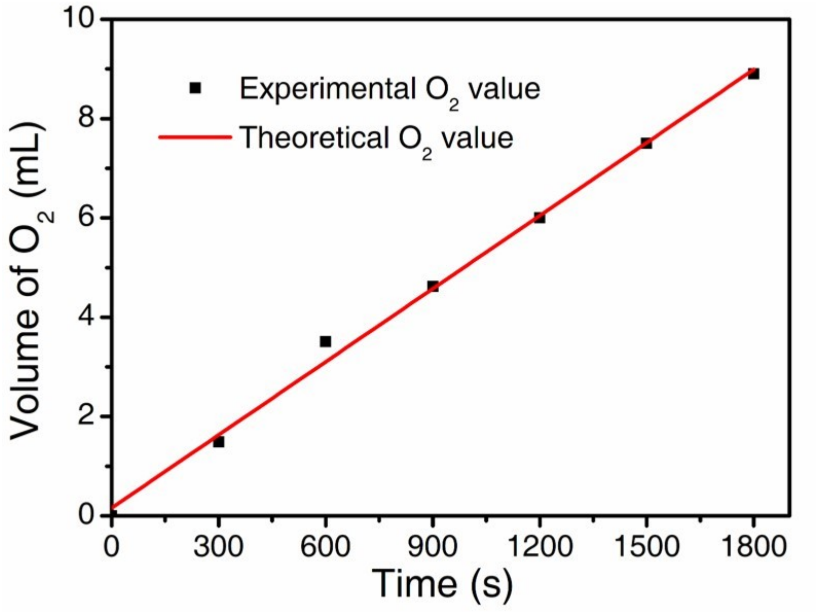

**Fig. S9.** The comparison of theoretical and experimental oxygen volume to calculate the Faradaic efficiency of $Co_{1/2}Ni_{1/2}$-CA.

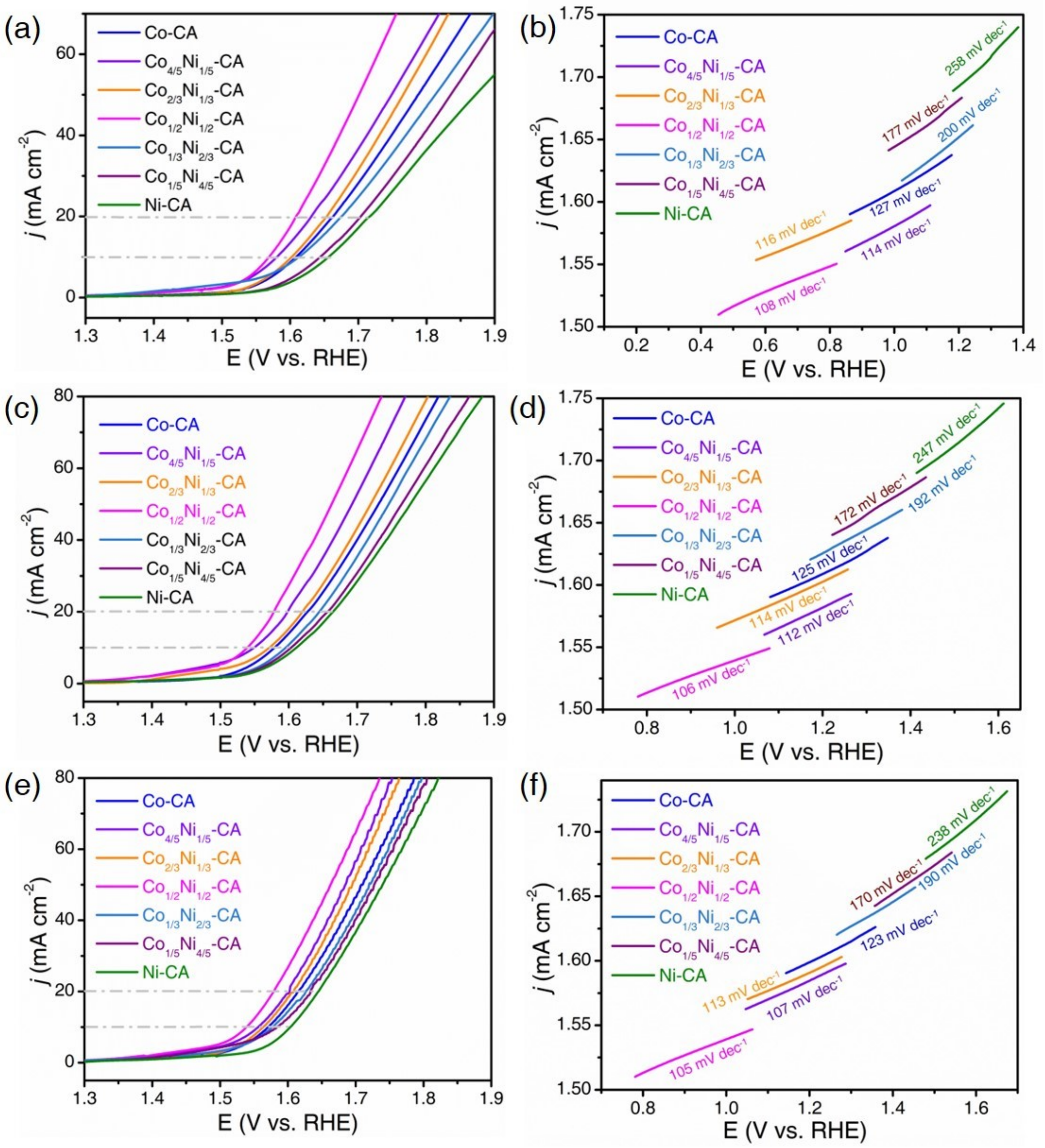

**Fig. S10.** LSV curves (a, c, e) and Tafel plots (b, d, f) of $Co_xNi_{1-x}$-CAs (x = 1, 4/5, 2/3, 1/2, 1/3, 1/5, 0) at 35 °C, 45 °C and 55 °C.

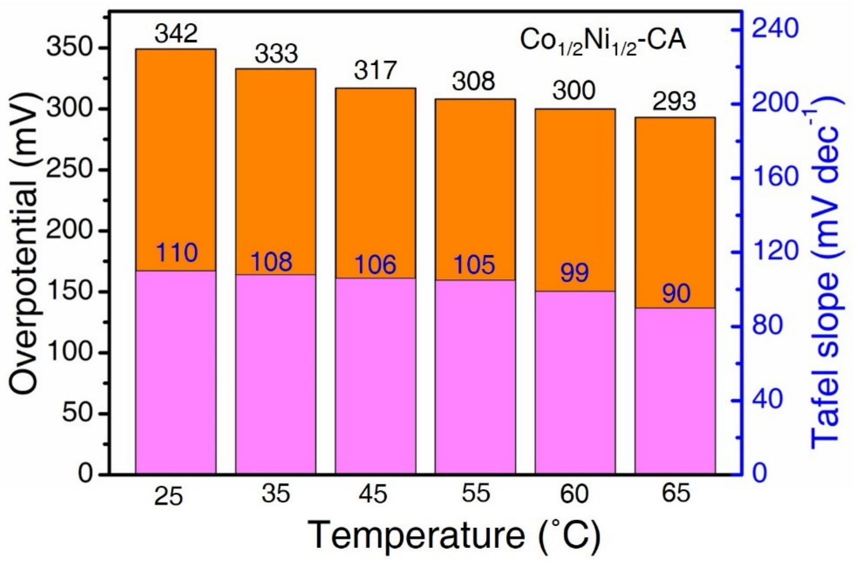

**Fig. S11.** Comparison on overpotential at 10 mA cm$^{-2}$ and Tafel slopes of $Co_{1/2}Ni_{1/2}$-CA at 25 °C, 35 °C, 45 °C, 55 °C, 60 °C and 65 °C in 1 M KOH solution.

**Table S3** Comparison of the OER performance of $Co_{1/2}Ni_{1/2}$-CA with other reported coordination polymers.

| Catalyst | η@10 mA $cm^{-2}$ (mV) | Tafel slope (mV $dec^{-1}$) | Solution | Ref. |
|---|---|---|---|---|
| $Co_{1/2}Ni_{1/2}$-CA | 349 | 110 | 1 M KOH | This work |
| $[Co(bpy)(fa)]_n(DMF)_{0.25}(bpy)_{0.25}$ | 382 | 84 | 1 M $KNO_3$ | [S3] |
| $[Co_3(HHTP)_2]_n$ LB nanosheets | 490 | 83 | 0.1 M KOH | [S4] |
| Co/Cu-MOF(3) | 395 | 94 | 1 M KOH | [S5] |
| UTSA-16 | 408 | 77 | 1 M KOH | [S6] |
| HE-MOF-RT | 245 | 54 | 1 M KOH | [S7] |
| NNU-23 | 365 | 81.8 | 0.1 M KOH | [S8] |
| NiCo-BTC | 335 | 56 | 1.0 M KOH | [S9] |
| PDA-MOF-0.1 | 350 | 66.1 | 1.0 M KOH | [S10] |
| Co Tp 3:1(Ni) | 371 | 53.6 | 1.0 M KOH | [S11] |
| MOF 2 | 389 | 108 | 1.0 M KOH | [S12] |
| Ni-MOFs | 415 | 93 | 1.0 M KOH | [S13] |
| $Ni(PyCHO)Cl_2$ | 356 | 79 | 1.0 M KOH | [S14] |
| $CoIITP[Co^{III}C]_2$ 3 | 412 | 63.6 | 1.0 M KOH | [S15] |
| Ni-BDC-1R | 225 | 89 | 1.0 M KOH | [S16] |
| Ni-BDC-3R | 332 | 132 | 1.0 M KOH | [S16] |
| CoCd-MOF | 353 | 123 | 1.0 M KOH | [S17] |
| Co-MOF-C | 342 | 119 | 1.0 M KOH | [S18] |
| $Co_{1/2}Ni_{1/2}$-HIPA | 367 | 115 | 1.0 M KOH | [S19] |
| Co/Cu-MOF | 395 | 94 | 1.0 M KOH | [S20] |
| Co-BDC | 392 | 77.2 | 1.0 M KOH | [S21] |
| Co-BPDC | 428 | 78.8 | 1.0 M KOH | [S21] |
| $Co_{2/3}Ni_{1/3}$-MOF | 325 | 86 | 1.0 M KOH | [S22] |

**Table S4** TOF of $Co_xNi_{1-x}$-CAs (x = 1, 4/5, 2/3, 1/2, 1/3, 1/5, 0) at different temperatures.

| catalyst | 25 °C | 35 °C | 45 °C | 55 °C |
|---|---|---|---|---|
| Co-CA | 0.011 | 0.016 | 0.035 | 0.062 |
| $Co_{4/5}Ni_{1/5}$-CA | 0.020 | 0.032 | 0.041 | 0.059 |
| $Co_{2/3}Ni_{1/3}$-CA | 0.019 | 0.027 | 0.046 | 0.047 |
| $Co_{1/2}Ni_{1/2}$-CA | 0.025 | 0.033 | 0.049 | 0.074 |
| $Co_{1/3}Ni_{2/3}$-CA | 0.011 | 0.015 | 0.022 | 0.046 |
| $Co_{1/5}Ni_{4/5}$-CA | 0.010 | 0.017 | 0.028 | 0.052 |
| Ni-CA | 0.001 | 0.002 | 0.008 | 0.014 |

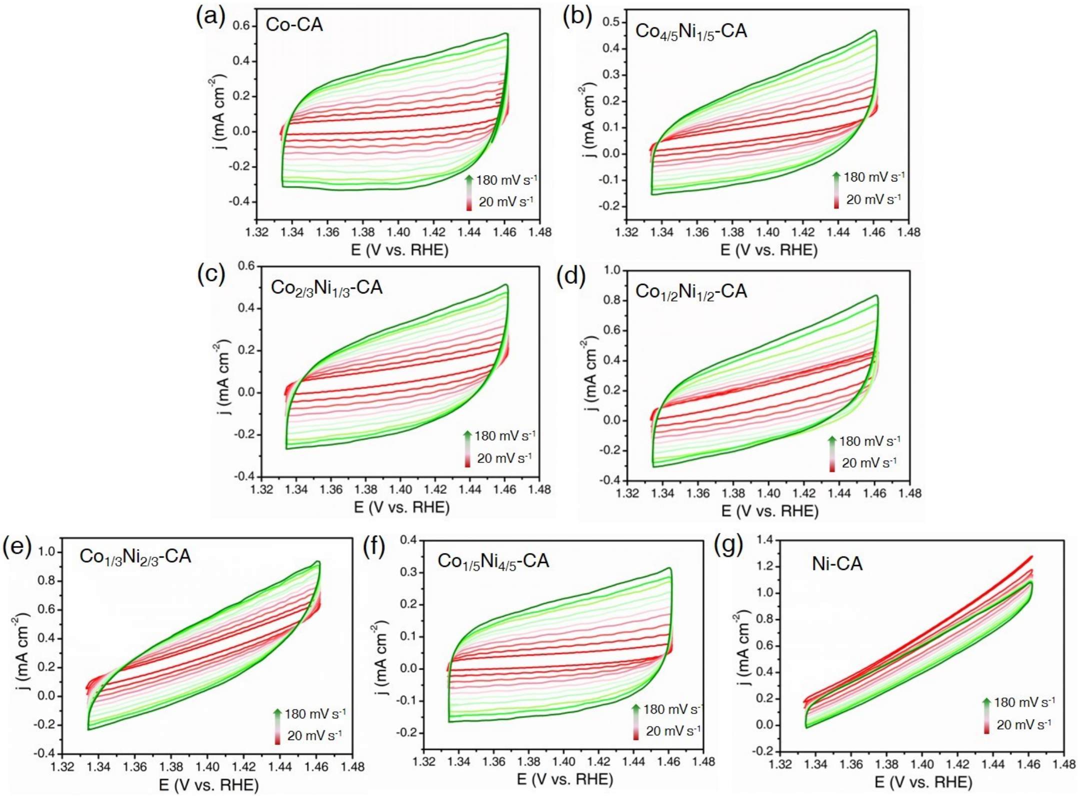

**Fig. S12.** CV curves of Co-CA (a), $Co_{4/5}Ni_{1/5}$-CA (b), $Co_{2/3}Ni_{1/3}$-CA (c), $Co_{1/2}Ni_{1/2}$-CA (d), $Co_{1/3}Ni_{2/3}$-CA (e), $Co_{1/5}Ni_{4/5}$-CA (f) and Ni-CA (g) at 35 °C.

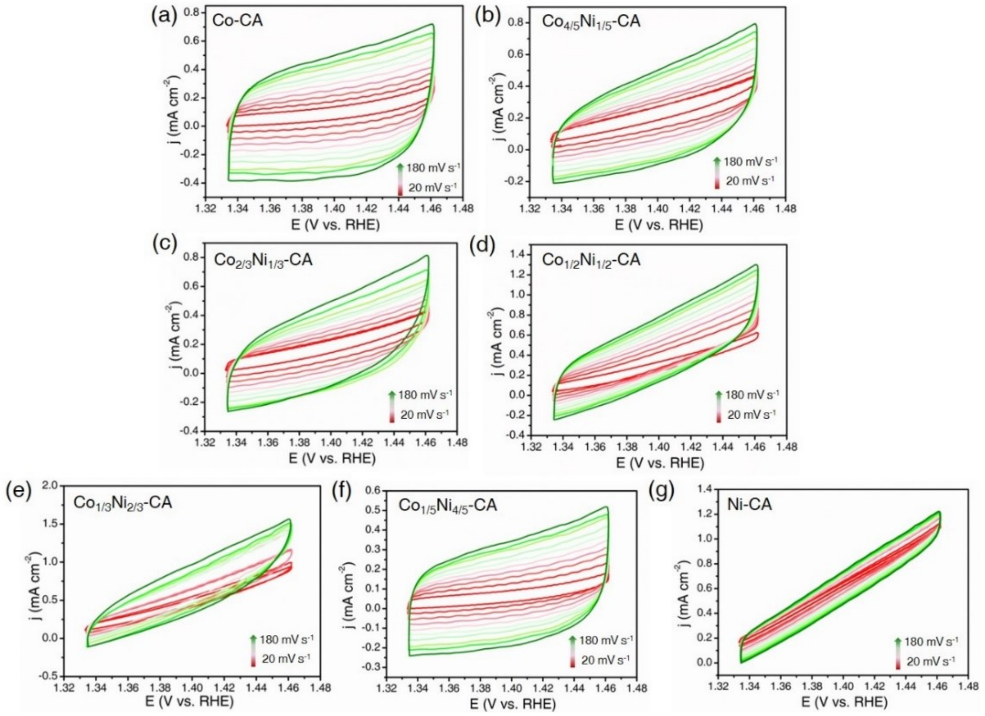

**Fig. S13.** CV curves of Co-CA (a), $Co_{4/5}Ni_{1/5}$-CA (b), $Co_{2/3}Ni_{1/3}$-CA (c), $Co_{1/2}Ni_{1/2}$-CA (d), $Co_{1/3}Ni_{2/3}$-CA (e), $Co_{1/5}Ni_{4/5}$-CA (f) and Ni-CA (g) at 45 °C.

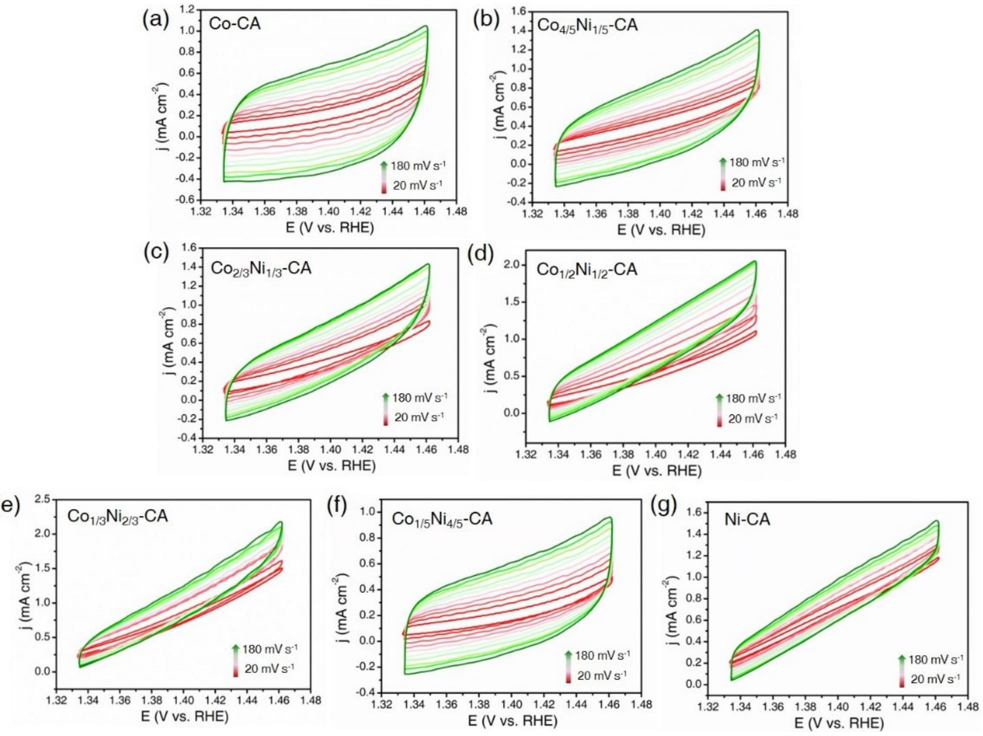

**Fig. S14.** CV curves of Co-CA (a), $Co_{4/5}Ni_{1/5}$-CA (b), $Co_{2/3}Ni_{1/3}$-CA (c), $Co_{1/2}Ni_{1/2}$-CA (d), $Co_{1/3}Ni_{2/3}$-CA (e), $Co_{1/5}Ni_{4/5}$-CA (f) and Ni-CA (g) at 55 °C.

**Table S5** $C_{dl}$ of $Co_xNi_{1-x}$-CAs (x = 1, 4/5, 2/3, 1/2, 1/3, 1/5, 0) at different temperatures.

| catalyst | 25 °C | 35 °C | 45 °C | 55 °C |
|---|---|---|---|---|
| Co-CA | 2.20 | 2.37 | 2.79 | 3.13 |
| $Co_{4/5}Ni_{1/5}$-CA | 2.93 | 3.10 | 3.43 | 4.03 |
| $Co_{2/3}Ni_{1/3}$-CA | 2.51 | 2.74 | 2.88 | 3.41 |
| $Co_{1/2}Ni_{1/2}$-CA | 3.01 | 3.56 | 4.29 | 5.17 |
| $Co_{1/3}Ni_{2/3}$-CA | 1.77 | 1.82 | 2.77 | 3.08 |
| $Co_{1/5}Ni_{4/5}$-CA | 0.76 | 1.37 | 2.64 | 2.99 |
| Ni-CA | 0.59 | 1.07 | 1.29 | 1.82 |

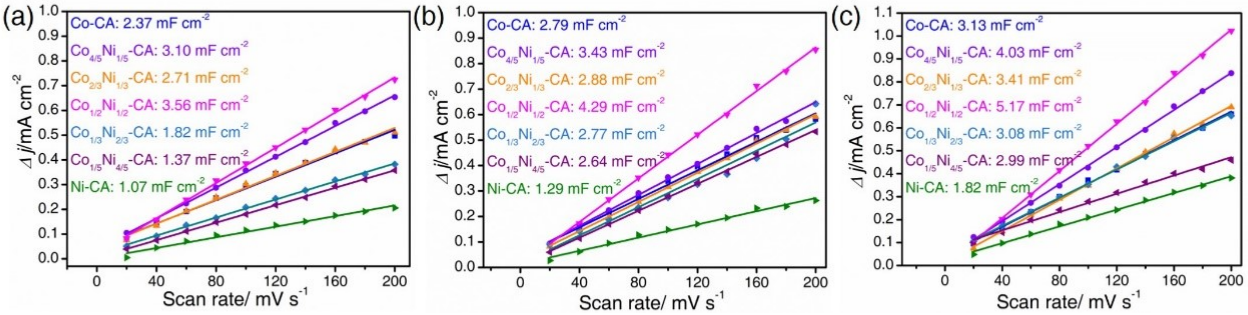

**Fig. S15.** $C_{dl}$ (a-c) of $Co_xNi_{1-x}$-CAs (x = 1, 4/5, 2/3, 1/2, 1/3, 1/5, 0) at 35 °C, 45 °C and 55 °C.

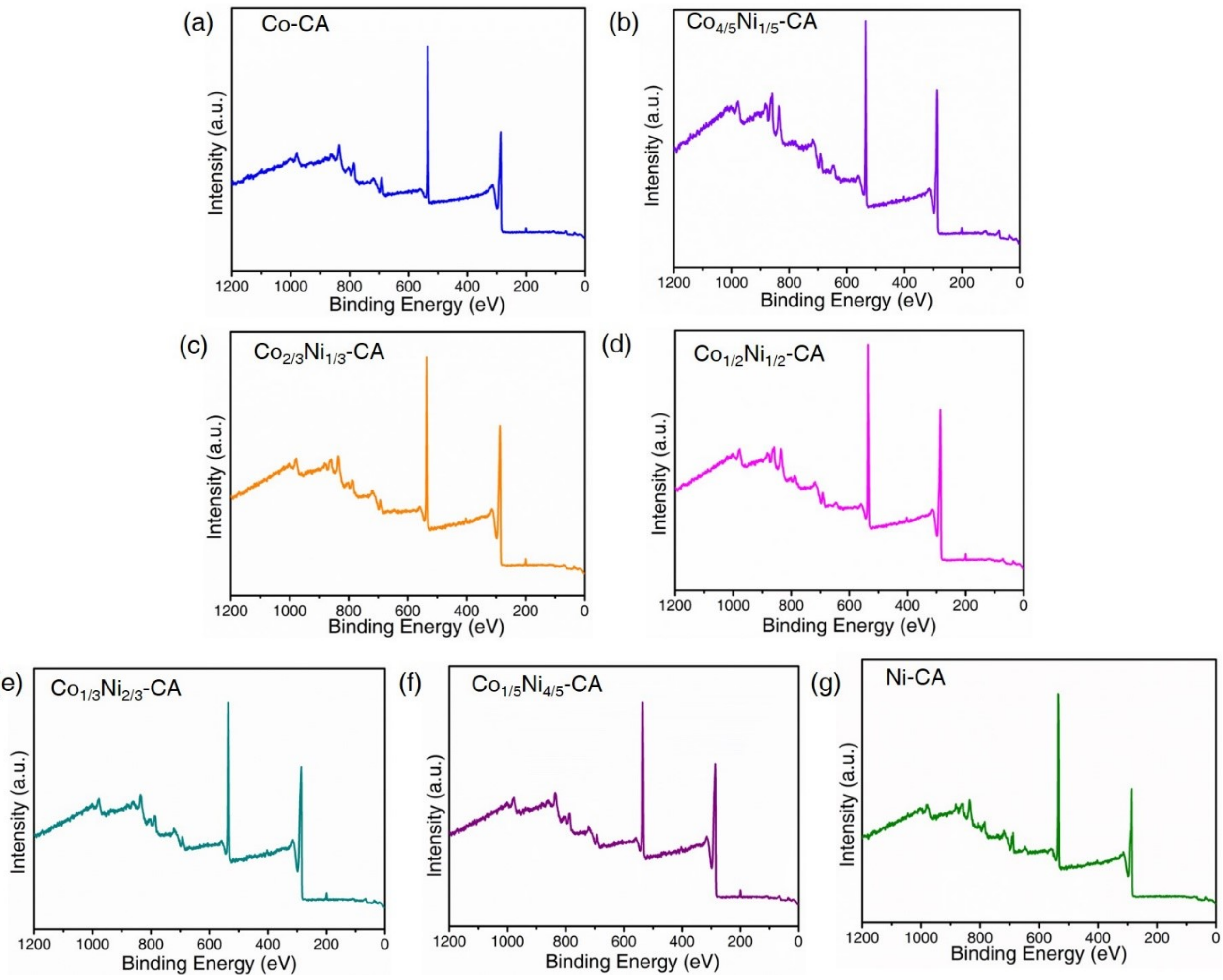

**Fig. S16.** XPS surveys of Co-CA (a), $Co_{4/5}Ni_{1/5}$-CA (b), $Co_{2/3}Ni_{1/3}$-CA (c), $Co_{1/2}Ni_{1/2}$-CA (d) $Co_{1/3}Ni_{2/3}$-CA (e), $Co_{1/5}Ni_{4/5}$-CA (f) and Ni-CA (g).

**Table S6** Binding energies of Co 2p and Ni 2p for Co-CA, $Co_{4/5}Ni_{1/5}$-CA, $Co_{2/3}Ni_{1/3}$-CA, $Co_{1/2}Ni_{1/2}$-CA, $Co_{1/3}Ni_{2/3}$-CA, $Co_{1/5}Ni_{4/5}$-CA and Ni-CA.

| Sample | Binding energy | | | |
|---|---|---|---|---|
| | Co $2p_{3/2}$ (eV) | Co $2p_{1/2}$ (eV) | Ni $2p_{3/2}$ (eV) | Ni $2p_{1/2}$ (eV) |
| Co-CA | 779.1 | 794.6 | --- | --- |
| $Co_{4/5}Ni_{1/5}$-CA | 778.9 | 794.4 | 853.9 | 871.4 |
| $Co_{2/3}Ni_{1/3}$-CA | 778.8 | 794.5 | 853.8 | 871.5 |
| $Co_{1/2}Ni_{1/2}$-CA | 778.8 | 794.5 | 853.8 | 871.6 |
| $Co_{1/3}Ni_{2/3}$-CA | 778.9 | 794.4 | 853.8 | 871.6 |
| $Co_{1/5}Ni_{4/5}$-CA | 778.8 | 794.4 | 853.6 | 871.3 |
| Ni-CA | --- | --- | 853.6 | 871.3 |

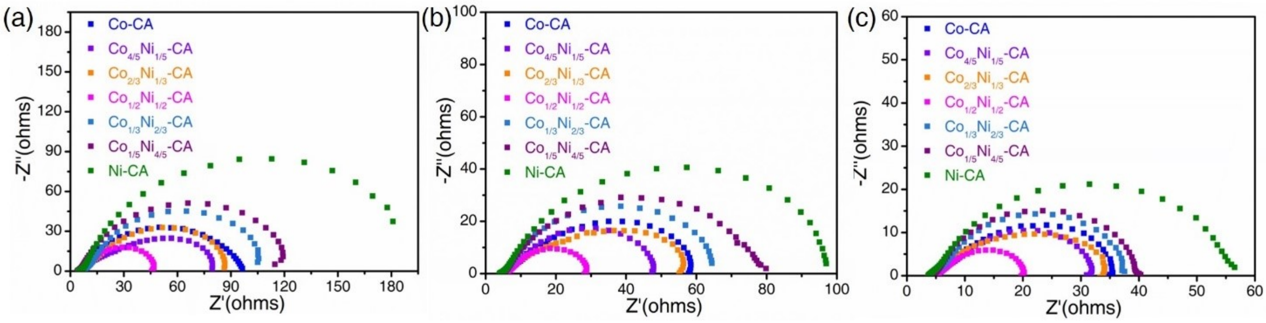

**Fig. S17.** EIS (a-c) of $Co_xNi_{1-x}$-CA (x = 1, 4/5, 2/3, 1/2, 1/3, 1/5, 0) at 35 °C, 45 °C and 55 °C.

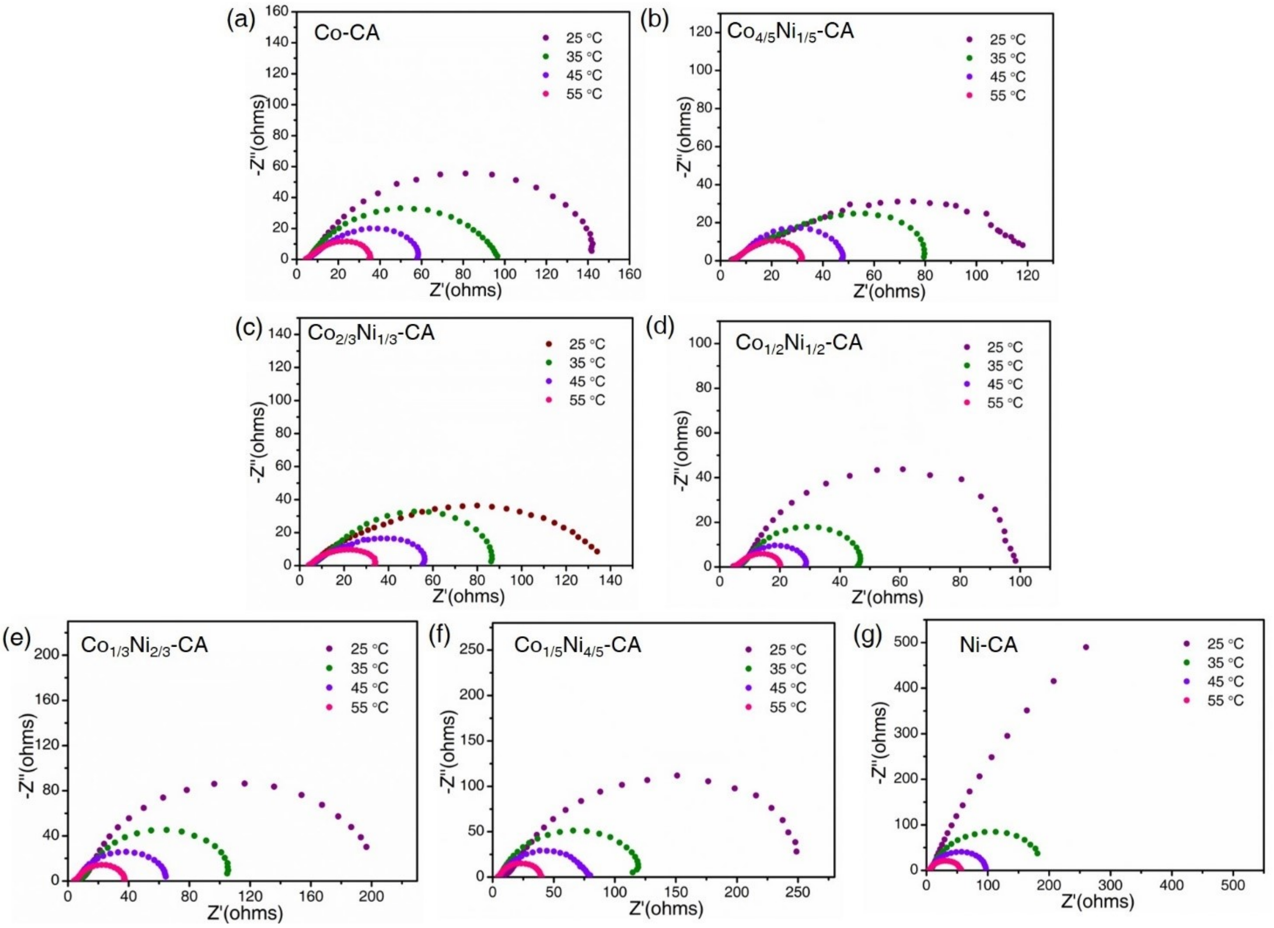

**Fig. S18.** The Nyquist curves of Co-CA (a), Co$_{4/5}$Ni$_{1/5}$-CA (b), Co$_{2/3}$Ni$_{1/3}$-CA (c), Co$_{1/2}$Ni$_{1/2}$-CA (d) Co$_{1/3}$Ni$_{2/3}$-CA, (e) Co$_{1/5}$Ni$_{4/5}$-CA (f) and Ni-CA (g) at different temperatures.

**Table S7** Charge transfer impedance ($R_{ct}$), activation energy ($E_a$) of Co$_x$Ni$_{1-x}$-CA at different temperatures.

| Sample | $R_{ct}$ (Ohm) | | | | $E_a$ (kJ mol$^{-1}$) |
|---|---|---|---|---|---|
| | 25 °C | 35 °C | 45 °C | 55 °C | |
| Co-CA | 141 | 96 | 57 | 35 | 59.68 |
| Co$_{4/5}$Ni$_{1/5}$-CA | 118 | 79 | 47 | 31 | 27.57 |
| Co$_{2/3}$Ni$_{1/3}$-CA | 134 | 86 | 55 | 33 | 25.07 |
| Co$_{1/2}$Ni$_{1/2}$-CA | 98 | 45 | 28 | 19 | 19.91 |
| Co$_{1/3}$Ni$_{2/3}$-CA | 196 | 104 | 64 | 37 | 52.36 |
| Co$_{1/5}$Ni$_{4/5}$-CA | 248 | 114 | 79 | 40 | 64.58 |
| Ni-CA | 482 | 180 | 96 | 56 | 69.49 |

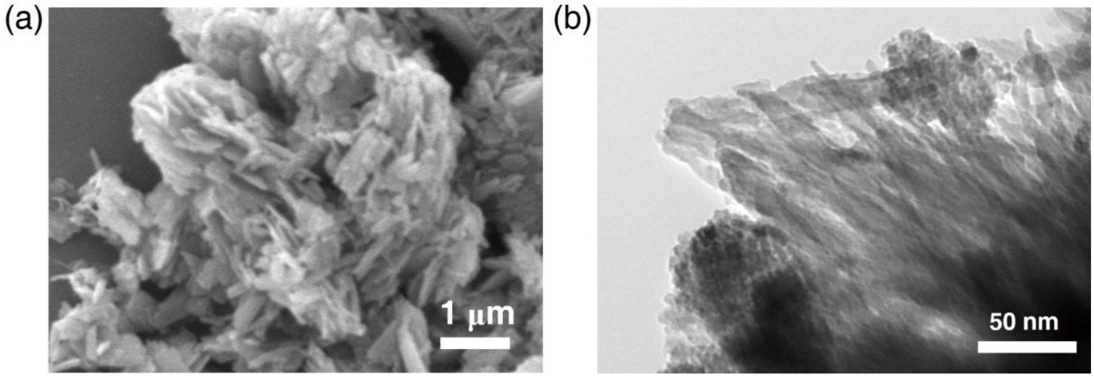

**Fig. S19.** The SEM image and TEM image of $Co_{1/2}Ni_{1/2}$-CA after 1000 CV cycles.

## References

[S1] S. Kawata, S. Kitagawa, H. Kumagai, T. Ishiyama, K. Honda, H. Tobita, K. Adachi, M. Katada. Chem. Mater. 1998, 10, 3902-3912.

[S2] J. Montero, D. Arenas-Esteban, D. Avila-Brande, E. Castillo-Martínez, S. Licoccia, J. Carretero-Gonzalez. Electrochim. Acta, 2020, 341, 136063.

[S3] M. Batoola, S. Ibrahima, B. Iqbala, S. Alib, A. Badshaha, S. Abbasb, D. R. Turnerc, M. A. Nadeem, Electrochim. Acta 2019, 298, 248-253.

[S4] M. Zhang, B.-H. Zheng, J. Xu, N. Pan, J. Yu, M. Chen, H. Cao, Chem. Commun. 2018, 54, 13579-13582.

[S5] Q. Qiu, T. Wang, L. Jing, K. Huang, D. Qin, Int. J. Hydrogen Energ. 2020, 45, 11077-11088.

[S6] J. Jiang, L. Huang, X. Liu, L. Ai, ACS Appl. Mater. Interfaces 2017, 8, 7193-7201.

[S7] X. Zhao, Z. Xue, W. Chen, X. Bai, R. Shia, T. Mu, J. Mater. Chem. A 2019, 7, 26238-26242.

[S8] X.-L. Wang, L.-Z. Dong, M. Qiao, Y.-J. Tang, J. Liu, Y. Li, S.-L. Li, J.-X. Su, Y.-Q. Lan, Angew. Chem. Int. Ed. 2018, 57, 9660-9664.

[S9] X. Zhang, J. Luo, K. Wan, D. Plessers, B. Sels, J. Song, L. Chen, T. Zhang, P. Tang, J. R. Morante, J. Arbiol, J. Fransaer, J. Mater. Chem. A 2019, 7, 1616.

[S10] F. Shi, Z. Wang, K. Zhu, X. Zhu and W. Yang, Electrochimica Acta 2022, 416, 140217.

[S11] S. Sprengel, M. Amiri, A. Bezaatpour, S. Nouhi, S. Baues, G. Wittstock and M. Wark, J. Electrochem. Soc. 2022, 169, 117509.

[S12] A. Joshi, A. Gaur, P. Sood and M. Singh, Inorg. Chem. 2021, 60, 12685-12690.

[S13] X. Ma, D. J. Zheng, S. Hou, S. Mukherjee, R. Khare, G. Gao, Q. Ai, B. Garlyyev, W. Li, M. Koch, J. Mink, Y. S. Horn, J. Warnan, A. S. Bandarenka, R. A. Fischer, ACS Catal. 2023, 13, 7587-7596.

[S14] Y. Wang, Z. Zhou, Y. Lin, Y. Zhang, Peiyan Bi, Q. Jing, Y. Luo, Z. Sun, J. Liao, Z. Gao, Chem. Eng. J. 2023, 462, 142179.

[S15] A. Aljabour, H. Awada, L. Song, H. Sun, S. Offenthaler, F. Yari, M. Bechmann, M. C. Scharber, W. Schöfberger, Angew. Chem. Int. Ed. 2023, 62, e202302208.

[S16] L. Zhang, J. Wang, K. Jiang, Z. Xiao, Y. Gao, S. Lin, B. Chen, Angew. Chem. Int. Ed. 2022, 61, e202214794.

[S17] K. Maity, K. Bhunia, D. Pradhan, K. Biradha, ACS Appl. Mater. Inter. 2017, 9, 37548-37553.

[S18] J. Du, F. Zhang, L. Jiang, Z. Guo, H. Song, Inorg. Chem. Commun. 2023, 158, 111661.

[S19] Lu, L.; Li, Q.; Du, J.; Shi, W.; Cheng, P. Chin. Chem. Lett. 2022, 33, 2928-2932.

[S20] Qiu, Q.; Wang, T.; Jing, L. Huang, K. Qin, D. Int. J. Hydrogen Energ. 2020, 45, 11077-11088.

[S21] Q. Zha, F. Yuan, G. Qin, Y. Ni. Inorg. Chem. 2020, 2, 1295-1305.

[S22] Q. Li, L. Lu, J. Liu, W. Shi, P. Cheng. J. Energy Chem. 2021, 63, 230-238.